Available online at www.sciencedirect.com
ScienceDirect
Energy Reports 9 (2023) 951–961
www.elsevier.com/locate/egyr

2022 The 3rd International Conference on Power and Electrical Engineering (ICPEE 2022)
29–31 December, Singapore

DC grid load flow solution incorporating generic DC/DC converter topologies

Zahid Javid, Ulas Karaagac*, Ilhan Kocar, Tao Xue

Department of Electrical Engineering, The Hong Kong Polytechnic University, Hung Hom, Kowloon, Hong Kong

Received 18 April 2023; accepted 20 May 2023
Available online 7 June 2023

Abstract

This research proposes a load flow (LF) solver with DC/DC converter models for DC distribution. The solver is based on modified-augmented-nodal-analysis (MANA) formulation and is implemented with the Newton–Raphson (NR) algorithm. The conditions to guarantee the convergence range of the MANA are demonstrated with Kantorovich's theorem. The proposed formulation is generic and flexible, allowing it to accommodate any arbitrary DC grid configuration. In addition, the formulation is extendable due to MANA's modular structure, which enables the incorporation of any device without changing the prior formulation. Instead of bus power injections, the summation of line flows and their associated derivatives are used when considering connections with various kinds of buses equipped with various converters. The proposed method is implemented in MATLAB and tested on the modified IEEE 33 bus distribution test feeder. Electromagnetic Transient (EMT) simulations confirmed the accuracy of the proposed method. Moreover, the results are also compared with the recently proposed efficient Laplacian Matrix (eLM) based method. Results suggest that the proposed method is robust and offers superior convergence characteristics with a faster simulation speed.

Peer-review under responsibility of the scientific committee of the 3rd International Conference on Power and Electrical Engineering, ICPEE, 2022.

Keywords: DC distribution grids; Fast convergence; Modified augmented nodal analysis; Load flow analysis

1. Introduction

Recently, there has been an open debate on whether to use alternating current (AC) or direct current (DC) in distribution power systems [1]. The advent of transformers offered a simple and effective technique for regulating voltage levels of AC in the past. In contrast, DC technology was not mature enough to regulate voltage levels for transmission and distribution [2]. However, with recent developments in power electronics, it is technically and economically feasible to regulate DC voltage levels. Therefore, engineering solutions and methods need to be re-evaluated in parallel with technological advances in generation, transmission, and distribution. In fact, such

* Corresponding author.
E-mail address: ulas.karaagac@polyu.edu.hk (U. Karaagac).

https://doi.org/10.1016/j.egyr.2023.05.164

Peer-review under responsibility of the scientific committee of the 3rd International Conference on Power and Electrical Engineering, ICPEE, 2022.

re-evolution on paradigm shift has led to the efficient and cost-effective high voltage DC (HVDC) transmission system over long distances [3]. Three significant developments in the last two decades have led to increased interest in DC distribution networks [4–6]. First, solar photovoltaic (PV) prices have dropped dramatically [7]. Second, LED lighting has swept the globe, rendering traditional incandescent and fluorescent light bulbs obsolete [8]. Third, the shift away from fossil fuels in favor of more environmentally friendly and efficient methods for generating electricity.

In DC distribution systems (DCDSs), a converter that can operate in three distinct modes replaces the transformer: constant power (CP), constant voltage (CV) or constant current (CC) [9]. The converter supplies a constant power load (CPL) while operating in CP mode [10]. The CP mode of operation of the converter makes the load flow (LF) constraint nonlinear and non-convex, which requires an iterative LF routine for solution [11]. Moreover, the different operation of DC/DC converters presents new challenges in the LF calculations and should be addressed with up-to-date methods. LF is one of the most researched fields since the 1960s in AC grids. However, with the DCDSs' recent resurgence, LF analysis in DC grids has recently been investigated. In addition, the convergence of the LF method is not always guaranteed for nonlinear LF equations, an algorithm may converge to unrealistic results or diverge. Several LF techniques for DC grids have been presented in the literature, most of which have their origins in the AC type LF methods [12–14]. Ref. [15] proposed an iterative LF solution method for DCDSs based on Laplacian matrix (LM) formulation using graph theory. This method has topology constraints, i.e., solving a meshed network requires an extra matrix. This study was further extended, where an improved LM (ILM) was employed to improve the simulation speed of the method [16]. These investigations also established the criterion for evaluating the convergence of the LF solver. Linear LF solvers based on Taylor and Laurent series expansion for DCDSs were also reported in the literature [17,18]. A thorough review and comparison of LF solvers for DCDSs can be found in [12,13]. None of the above studies considered DC/DC converters in LF formulation.

The DC/DC converter models in the LF equations have been the subject of just one recent study [19], which is an extended version of the study presented in [16] using efficient LM (eLM). Additionally, none of the aforementioned research used derivative-based approaches, and their convergence is slower than derivative-based methods [20]. Authors in [20] used a modified augmented nodal analysis (MANA) approach to solve a DCDS. The MANA formulation approach works with any kind of network topology and can easily be modified to incorporate new types of network components. It aids in avoiding numerous theoretical issues by providing a systematic means of deriving the Jacobian matrix terms [21–23]. The MANA approach yielded the best simulation performance and fastest convergence times. Around 30%, 42%, and 88% faster simulation speeds have been achieved compared to ILM [16], LM [15], and GS LF solvers, respectively [20]. In addition, the classical NR method may have convergence issues due to non-linear and non-convex LF equations, but with MANA implementation, convergence characteristics can be strengthened [21]. The disadvantages of traditional nodal analysis (NA) can be found in [24].

The primary objective of this study is to formulate an LF algorithm for DCDSs that can accomplish fast convergence while ensuring the uniqueness of the solution. This article expanded the DC-MANA formulation to include DC/DC converter models within the LF equations. The following is a list of the paper's principal contributions:

- Reformulation of DC-MANA to incorporate different converter models into LF equations.
- Generalization of the proposed approach so that it can handle any DCDS configuration.
- The demonstration of the uniqueness of the solution with Kantorovich's theorem.

The results are compared with the existing methodology in terms of processing time and the number of required iterations [19]. The rest of this paper is laid out as follows. The DC/DC converter models and associated line flow equations are presented in Section 2. Section 3 contains the reformulation of the MANA to incorporate converter models. Simulation results and discussion are presented in Section 4. The conclusions are drawn in Section 5.

2. DC/DC converter models and line flows equations

Typically, DC/DC converters are for voltage regulation, however, additional controls like, CC, CP, and constant duty cycle are possible with DC/DC converters. We assumed continuous conduction mode operation when the converter's conductance is larger than the critical value. In this study, we considered Buck, Boost, and Buck-Boost converters. Fig. 1 depicts a steady-state model of a DC-to-DC converter. The arrow on the top of the duty cycle in

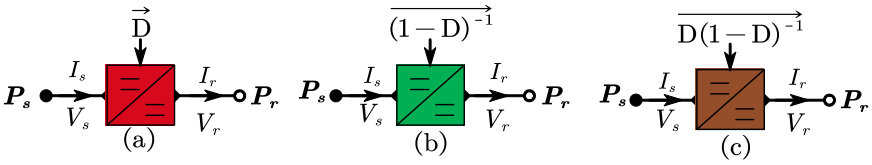

Fig. 1. DC/DC converters (steady-state) (a) Buck operation; (b) Boost operation; (c) Buck-Boost operation.

Fig. 1 shows the direction of power flow through converter. The DC/DC converter's output voltage is dependent on the duty cycle ratio (D).

$$D = t_{on} \times (t_{on} + t_{off})^{-1} \tag{1}$$

Following are the input and output relationships for the buck converter.

$$V_r = DV_s \tag{2}$$

$$I_r = D^{-1} I_s \tag{3}$$

Subscripts "s" and "r" indicate sending and receiving end of the converter, respectively.
For boost operation, the input/ output relationship is as follows.

$$V_r = (1 - D)^{-1} V_s \tag{4}$$

$$I_r = (1 - D) I_s \tag{5}$$

The input/ output relationship for the buck-boost converter is given below.

$$V_r = D(1 - D)^{-1} V_s \tag{6}$$

$$i_r = D(1 - D) I_s \tag{7}$$

The output power of the converter is dependent on the efficiency of the converter (η_{conv}) as follows.

$$P_s = \eta_{conv}^{-1} P_r = \eta_{conv}^{-1} V_r I_r \tag{8}$$

2.1. DC line model

The LF equations can be extended to account for DC/DC converter operations by considering the DC line model shown in Fig. 2 . The conductance matrix needs modification to limit the same base voltage on both sides of the converter. If the converter operation is defined with a converter constant ξ, then the modified conductance matrix is as follows.

$$G_{sr} = \begin{bmatrix} \frac{G_{sr}}{\xi^2} & \frac{-G_{sr}}{\xi} \\ \frac{-G_{sr}}{\xi} & G_{sr} \end{bmatrix} \tag{9}$$

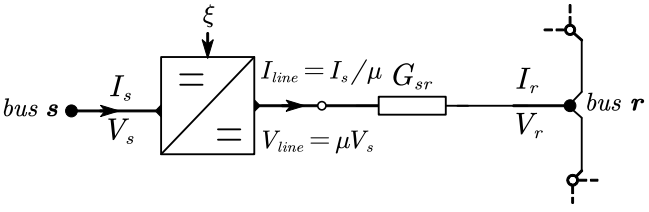

Fig. 2. DC line model connected with a DC/DC converter.

To express the per unit (*p.u.*) relationship between the voltages on either side of the converter, we can write the following expression.

$$V_{r,p.u} = \xi V_{s,p.u} \tag{10}$$

The DC line current is given as follows.

$$I_{line} = G_{sr}(\xi V_{s,pu} - V_{r,pu}) \tag{11}$$

The equation for the line joining bus s and bus r can be derived from (8), (10), and (11).

$$P_{sr} = G_{sr}(\alpha_s \eta_{sr}^{-1} + \beta_s \eta_{rs}) \left((\xi V_{s,pu})^2 - \xi V_{s,pu} V_{r,pu}\right) \tag{12}$$

where, α_s and β_s are the converters efficiency parameters connected with bus s, and it is dependent on the direction of the power flow as follows.

$$\begin{cases} \alpha_s = 1; & \beta_s = 0\ ; & if & \xi V_s > V_r : \eta_{sr} \\ \alpha_s = 0; & \beta_s = 1\ ; & if & \xi V_s < V_r : \eta_{rs} \\ \alpha_s = 0.5; & \beta_s = 0.5; & if & \xi V_s = V_r : \eta_{sr}\ ,\ \eta_{rs} \end{cases} \tag{13}$$

The converter constant ξ is replaced with respect to the converter mode of operation, e.g., for buck converter ξ = D. From now onwards the unit of measure will be in per unit, and the subscript "$p.u$". will no longer be used.

2.2. Line flows

Potential DC bus interconnections are illustrated in Fig. 3. Since the sending bus could be connected to the receiving bus in several different ways, the sum of line flows is developed as contrasted to bus power injections, which is a common practice in conventional LF formulation.

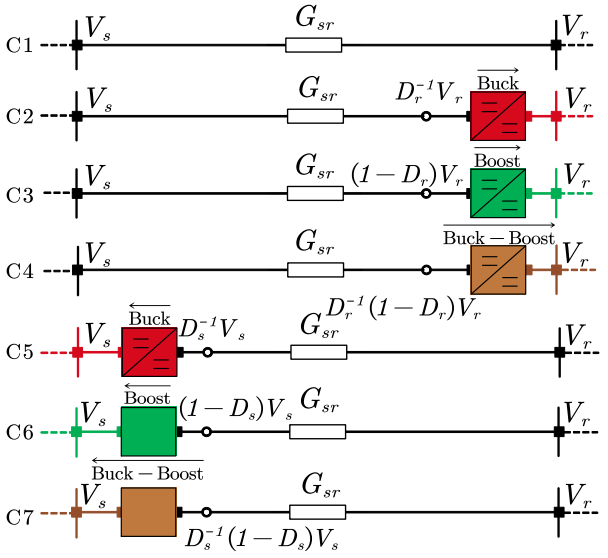

Fig. 3. Possible interconnections between DC buses.

The line flows from the sending bus side can be written as follows.

$$P_{sr}^{C1} = G_{sr}(V_s^2 - V_s V_r) \tag{14}$$
$$P_{sr}^{C2} = G_{sr}(V_s^2 - V_s V_r D_r^{-1}) \tag{15}$$
$$P_{sr}^{C3} = G_{sr}[V_s^2 - V_s V_r(1 - D_r)] \tag{16}$$
$$P_{sr}^{C4} = G_{sr}[V_s^2 - V_s V_r(D_r^{-1}(1 - D_r))] \tag{17}$$
$$P_{sr}^{C5} = G_{sr}[V_s^2 D_s^{-2} - V_s V_r D_s^{-1}]\{\alpha_s \eta_{sr}^{-1} + \beta_s \eta_{rs}\} \tag{18}$$
$$P_{sr}^{C6} = G_{sr}[V_s^2(1 - D_s)^2 - V_s V_r(1 - D_s)]\{\alpha_s \eta_{sr}^{-1} + \beta_s \eta_{rs}\} \tag{19}$$
$$P_{sr}^{C7} = G_{sr}[V_s^2 D_s^{-2}(1 - D_s)^2 - V_s V_r D_s^{-1}(1 - D_s)]\{\alpha_s \eta_{sr}^{-1} + \beta_s \eta_{rs}\} \tag{20}$$

It is important to notice that (15) to (17) are derived from the sending end bus, so they do not contain converter efficiency parameters.

2.3. Partial derivatives

The partial derivatives of state variables of line flow for all the possible cases (C1-C7) are given below.

$$\partial P_{sr}^{C1}/V_s = G_{sr}(2V_s - V_r) \tag{21}$$
$$\partial P_{sr}^{C1}/V_r = G_{sr}(0 - V_r) \tag{22}$$
$$\partial P_{sr}^{C2}/\partial V_s = G_{sr}[2V_s - V_r D_r^{-1}] \tag{23}$$
$$\partial P_{sr}^{C2}/\partial V_r = G_{sr}[0 - V_r D_r^{-1}] \tag{24}$$
$$\partial P_{sr}^{C3}/\partial V_s = G_{sr}[2V_s - V_r(1 - D_r)] \tag{25}$$
$$\partial P_{sr}^{C3}/\partial V_r = G_{sr}[0 - V_s(1 - D_r)] \tag{26}$$
$$\partial P_{sr}^{C4}/\partial V_s = G_{sr}[2V_s - V_r(D_r^{-1}(1 - D_r))] \tag{27}$$
$$\partial P_{sr}^{C4}/\partial V_r = G_{sr}[0 - V_s(D_r^{-1}(1 - D_r))] \tag{28}$$
$$\partial P_{sr}^{C5}/\partial V_s = G_{sr}[2V_s D_s^{-2} - V_r D_s^{-1}]\{\alpha_s \eta_{sr}^{-1} + \beta_s \eta_{rs}\} \tag{29}$$
$$\partial P_{sr}^{C5}/\partial V_r = G_{sr}[0 - V_s D_s^{-1}]\{\alpha_s \eta_{sr}^{-1} + \beta_s \eta_{rs}\} \tag{30}$$
$$\partial P_{sr}^{C5}/\partial D_s = G_{sr}[-2V_s^2 D_s^{-3} + V_s V_r D_s^{-2}]\{\alpha_s \eta_{sr}^{-1} + \beta_s \eta_{rs}\} \tag{31}$$
$$\partial P_{sr}^{C6}/\partial V_s = G_{sr}[2V_s(1 - D_s)^2 - V_r(1 - D_s)]\{\alpha_s \eta_{sr}^{-1} + \beta_s \eta_{rs}\} \tag{32}$$
$$\partial P_{sr}^{C6}/\partial V_r = G_{sr}[0 - V_s(1 - D_s)]\{\alpha_s \eta_{sr}^{-1} + \beta_s \eta_{rs}\} \tag{33}$$
$$\partial P_{sr}^{C6}/\partial D_s = G_{sr}[2V_s^2(1 - D_s)(0 - 1) - V_s V_r(0 - 1)]\{\alpha_s \eta_{sr}^{-1} + \beta_s \eta_{rs}\} \tag{34}$$
$$\partial P_{sr}^{C7}/\partial V_s = G_{sr}[2V_s D_s^{-2}(1 - D_s)^2 - V_r D_s^{-1}(1 - D_s)]\{\alpha_s \eta_{sr}^{-1} + \beta_s \eta_{rs}\} \tag{35}$$
$$\partial P_{sr}^{C7}/\partial V_r = G_{sr}[0 - V_s D_s^{-1}(1 - D_s)]\{\alpha_s \eta_{sr}^{-1} + \beta_s \eta_{rs}\} \tag{36}$$
$$\partial P_{sr}^{C7}/\partial D_s = G_{sr}[V_s^2\{-2D_s^{-3}(1 - D_s)^2 - 2D_s^{-2}(1 - D_s)\} - V_s V_r\{-1D_s^{-2}(1 - D_s) - D_s^{-1}\}]\{\alpha_s \eta_{sr}^{-1} + \beta_s \eta_{rs}\} \tag{37}$$

3. MANA formulation

After developing all required models and configurations, the stage is set now to introduce MANA for the DC LF solution. For a gentle introduction to MANA formulation for LF applications, readers are referred to [20,24,25]. MANA approach takes not only voltages but also currents of "non-constitutive elements" (NCE) as state variables (network elements with current expressions that are hard to write as a function of their terminal voltages alone). The MANA formulation can be summarized below.

$$F(u) = G_{aug}\, u + I_{cpt} - I_{gen} - K \tag{38}$$

where u is the vector of state variables, I_{cpt} and I_{gen} are the augmented vector of currents for constant power terminals (CPTs) and generator nodes, respectively, "K" is the vector of independent voltage sources and currents. G_{aug} is given below.

$$[G_{aug}] = \begin{bmatrix} G & A \\ B & D \end{bmatrix} \tag{39}$$

where G is the conductance matrix, A, B, and D are the matrices that represent the voltage–current relationship of the network components, which are not represented with their conductance model. following is the simplified rendition of MANA for a DCDS.

$$\begin{bmatrix} G_{aug} & C_{cpt}^T \\ C_{cpt} & 0 \end{bmatrix} \begin{bmatrix} V_s \\ I_{cpt} \end{bmatrix} = \begin{bmatrix} I_s \\ V_{cpt} \end{bmatrix} \tag{40}$$

where C is the connectivity matrix, its details can be found in [16, 26]. In (38), the slack bus is modeled as a voltage source. Like classical NA formulation, the constant resistive load (CRL) is directly incorporated in G_{aug}.

The presence of CPTs in the system makes LF equations non-linear and non-convex, so an iterative method is needed. We employ the NR algorithm to solve the proposed MANA formulation.

3.1. Bus types and method generalization

Table 1 presents the bus types (BTs) with associated known (✔) and unknown (✗) quantities used for realizing DC/DC DS LF formulation. Bus type 1 (BT-1) is a slack bus, bus type 2 (BT-2) is a load bus, bus type 3 (BT-3) is a voltage-controlled bus, and bus 4 (BT-4) is a voltage-controlled bus through a DC/DC converter.

Table 1. Type of buses in DCDS.

Bus (s)	Type	Vs	Ps	Ds	Bus (s)	Bus (s) type	Vs	Ps	Ds
1	Slack	✔	✗	–	3	Vdc	✔	✗	–
2	Pdc	✗	✔	–	4	Pdc-Vdc	✔	✗	✗

Finally, the vector of state variables (x) can be written as follows.

$$x = \begin{bmatrix} V_i & \cdots & D_j & \cdots \end{bmatrix}^T, \forall i \in BT-2, \forall j \in BT-4 \tag{41}$$

Please note that if the power limits of a DC voltage-controlled bus are violated, it will act as a DC load bus (P_{dc}) with active power equal to the violated limit, and the voltage magnitude of that bus becomes a variable in the unknown vector. To generalize the presented approach, binary variables are introduced, as shown in Table 2. In the formulation, the bar for binary elements stands for binary features that genuinely represent their binary complement.

Table 2. Binary variables and their values.

Variable	Type	Operation	Converter	No converter
B	bus type vector	buck	1	0
T	bus type vector	boost	1	0
BT	bus type vector	buck-boost	1	0
L	line type matrix	buck/ boost/ buck-boost	1	0

The potential interconnections of load (l) and generator (g) in a DC grid are illustrated in Fig. 4.

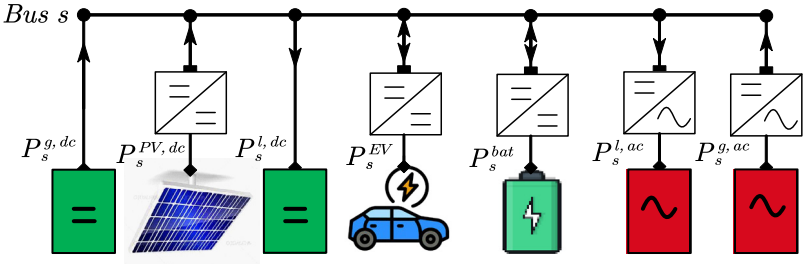

Fig. 4. Possible connection with DC bus.

A generalized expression for specified and calculated active power at sending bus "s" can be written as follows.

$$P_s^{sp} = [P_s^{g,dc} + \eta_{s,PV} P_s^{PV,dc} - P_s^{l,dc} - \tau \frac{P_s^{EV}}{\eta_{s,EV}} + \overline{\tau}\eta_{s,EV} P_s^{EV} - \mu \frac{P_s^{bat}}{\eta_{s,bat}} + \overline{\mu}\eta_{s,bat} P_s^{bat} + \eta_{s,rec} P_s^{g,ac} - \frac{P_s^{l,ac}}{\eta_{s,inv}}] \tag{42}$$

$$P_s^{cal} = \sum_{\substack{r=1 \\ r \neq s}}^{N} [C_{sr}] \left[\begin{array}{r} \overline{B}_s \overline{T}_s \overline{L}_{sr} \overline{B}_r \overline{\overline{T}}_r \left[P_{sr}^{C1}\right] + B_s \overline{T}_s L_{sr} \overline{B}_r \overline{\overline{T}}_r \left[P_{sr}^{C5}\right] + \overline{B}_s T_s L_{sr} \overline{B}_r \overline{\overline{T}}_r \left[P_{sr}^{C6}\right] + B_s T_s L_{sr} \overline{B}_r \overline{\overline{T}}_r \left[P_{sr}^{C7}\right] \\ \ldots + \overline{B}_s \overline{T}_s L_{sr} B_r \overline{\overline{T}}_r \left[P_{sr}^{C2}\right] + \overline{B}_s \overline{T}_s L_{sr} \overline{B}_r T_r \left[P_{sr}^{C3}\right] + \overline{B}_s \overline{T}_s L_{sr} B_r T_r \left[P_{sr}^{C4}\right] \end{array} \right] \tag{43}$$

where, τ, $\overline{\tau}$, μ, and $\overline{\mu}$: binary coefficients for charging and discharging for EVs and batteries respectively. N is no of buses in the system.

If λ defines the type of load : $\lambda = 0$: for CPL, $\lambda = 1$: for CCL, $\lambda = 2$: for CRL, then a generic expression for all load models is given below:

$$P_s^{(t)} = P_s^{sp} \times (V_s^{(t)} / V_s^{sp})^{\lambda} \tag{44}$$

3.2. Jacobian matrix formation and constraint equations

The Jacobian matrix in MANA formulation is given as follows:

$$\begin{bmatrix} G_{aug} & C_{cv}^T & C_{cpt} \\ C_{cv} & 0 & 0 \\ \frac{\partial \mho_L}{\partial V_L} & 0 & \frac{\partial \mho_L}{\partial I_L} \end{bmatrix}^{(t)} \begin{bmatrix} \Delta V_{cpt} \\ \Delta I_{cv} \\ \Delta I_L \end{bmatrix}^{(t)} = - \begin{bmatrix} \mho_{kcl} \\ \mho_{cv} \\ \mho_L \end{bmatrix}^{(t)} \tag{45}$$

$\mho_{kcl}$, $\mho_{cv}$ and $\mho_L$ are given as follows:

$$\mho_{kcl}^{(t)} = \begin{bmatrix} G_{aug} & C_{cv}^T & C_{cpt} \end{bmatrix} \begin{bmatrix} V_{cpt} & I_{cv} & I_L \end{bmatrix} - I_L \tag{46}$$

$$\mho_{cv}^{(t)} = C_{cv} \times V_{cpt}^{(t)} - V_{cv} \tag{47}$$

$$\mho_L^{(t)} = P^{sp} \left(\frac{V_L^{(t)}}{V_L^{sp}} \right)^{\lambda} - (V_L \times I_L)^{(t)} \tag{48}$$

The load constraint equation $\mho_L$ will remain the same for all type of loads. The generalized expression of partial derivatives for all type of load models are given below.

$$\frac{\partial \mho_L}{\partial V_L} = \frac{\lambda \times P^{sp} \times (V_L)^{\lambda - 2}}{V_L^{sp}} - I_L \tag{49}$$

$$\frac{\partial \mho_L}{\partial I_L} = -V_L \tag{50}$$

Finally, the mismatch vector can be written below.

$$F(x) = \quad P_s^{sp} - P_s^{cal} \quad , \quad \forall s \in N \tag{51}$$

3.3. Convergence

The convergence of the NR algorithm for a given initial condition can be investigated with Kantorovich's theorem. There are two parameters to test the convergence of the NR algorithm, as shown below.

$$\delta = \left[\rho \times (R_{thv})^2 (1 - \rho \times R_{thv}) \left(\rho + I_{cpt}^{(0)} \right) / \left(1 - 2\rho \times R_{thv} - I_{cpt}^{(0)} \times R_{thv} \right)^3 \right] < \sigma \tag{52}$$

where, σ is the boundary value of the given network as given in (53), ρ is the maximum loading, R_{thv} is the Thevenin equivalent resistance.

$$\left[\left(\rho + I_{cpt}^{(0)} \right) \times R_{thv} / (1 - \rho \times R_{thv}) \right] \leq \sigma < 1 \tag{53}$$

The detailed derivation and proof of σ and δ can be found in [20]. Only network parameters and demand conditions affect the expression (52). Before starting to perform the complete LF iterative operation under any load, the guaranteed convergence range can be estimated. The proposed method can guarantee convergence if $\delta < \sigma$ for a specific loading. By determining the contraction constant using the Banach fixed theorem (BFPT), one can probe the convergence properties of the eLM method [15,16]. The detailed derivation and proof of the contraction

constant can be found in [15]. The BFPT provides a mechanism for building fixed points of specific self-maps of metric spaces and guarantees their existence and uniqueness. Kantorovich's theorem is similar to BFPT, but it states existence and uniqueness of a zero rather than a fix point.

4. Results and discussion

The IEEE 33 bus test feeder, as depicted in Fig. 5, is used to validate the proposed formulation. The date of test feeder is taken from [15,19]. The Tolerance for convergence was set at 10 digits of precision. During the simulation, the load is increased to 2.5 times to the original load. All simulations were performed using MATLAB 2021b on a desktop PC with: CPU (Intel Core i7 @ 3.21 and 3.19 GHz), 16 GB RAM.

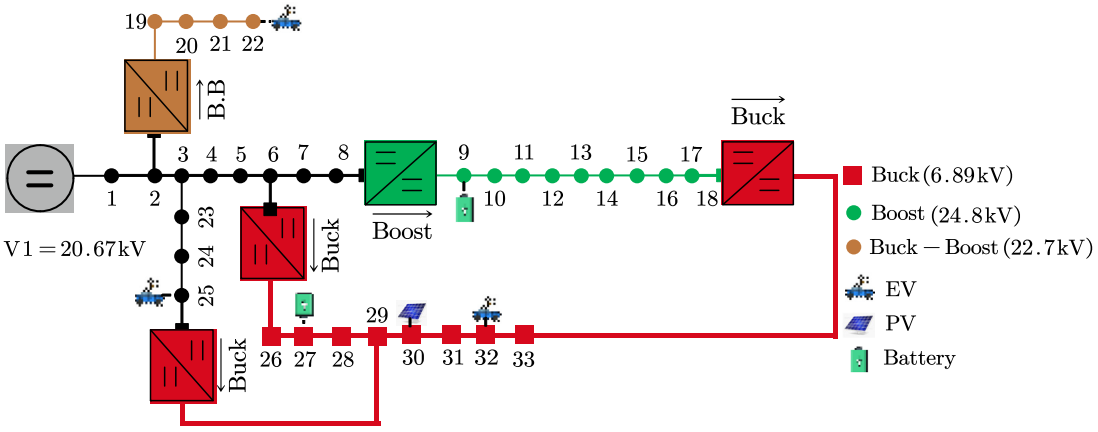

Fig. 5. Modified IEEE 33 node test feeder.

In order to verify the precision of the MANA method, the test network is also simulated using EMT. Fig. 6 depicts the voltage summary of the test network, which verifies the accuracy of the MANA method. Fig. 7 shows a relationship between error and number of iterations. The proposed technique is compared to the eLM considering CPU processing time and required iterations. Fig. 7 demonstrates that the proposed LF solver requires fewer iterations to attain the same level of accuracy. Moreover, under high-loading conditions, the performance of the proposed method is comparable to that of the eLM LF solver.

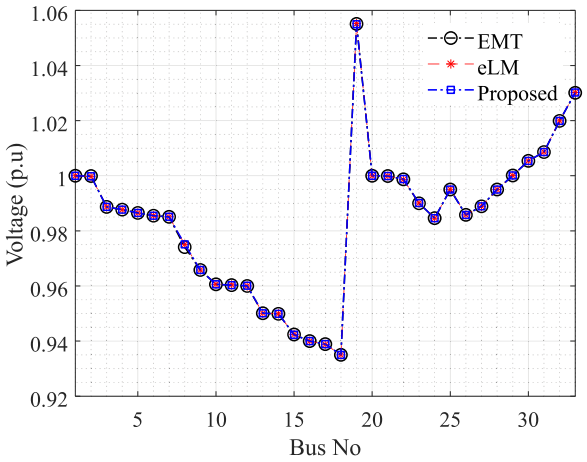

Fig. 6. Voltage profile.

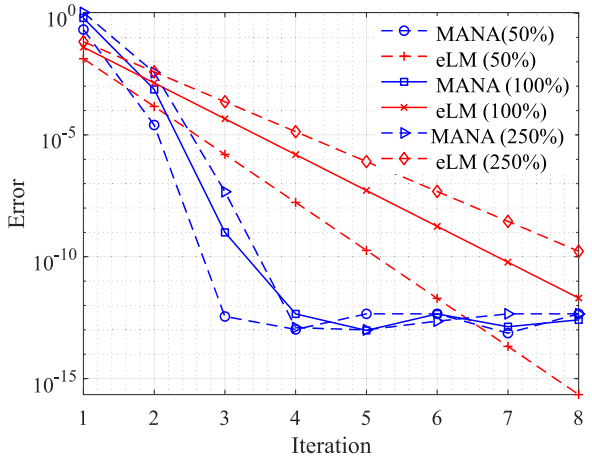

Fig. 7. Error versus number of iterations.

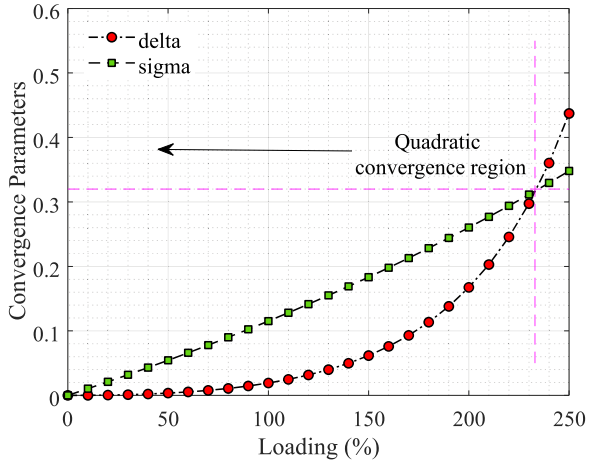

Fig. 8. Convergence parameters of MANA for different loadings.

4.1. Convergence characteristics of MANA and eLM

The proposed method's convergence is demonstrated using Kantorovich's theorem. The value of convergence parameters (σ and δ) is plotted in Fig. 8 at different loading conditions. The region where the proposed method can guarantee quadratic convergence is marked in Fig. 8. While the convergence of the eLM is demonstrated with BFPT by plotting the values of contraction of at different loadings as shown in Fig. 9. The eLM LF solver can assure convergence if the contraction constant's value is less than unity. It can be seen from the results that both LF methods provide a wide range of convergence. However, MAMA outperforms eLM in terms of convergence speed as MANA offers quadratic convergence, whereas the convergence of the eLM methods is linear.

Fig. 10 shows the processing time of MANA and eLM. Results show that MANA is much faster than the eLM LF solver. The improvements in time are 56%, 64% at the original loading, and 250% of the original loading, respectively.

4.2. Discussion on MANA vs. Classical nodal analysis

MANA formulation eliminates all limitations of classical NA and is ideal for symbolic and numerical analysis. MANA may seem to take more storage and computational time than classical NA. MANA can perform faster

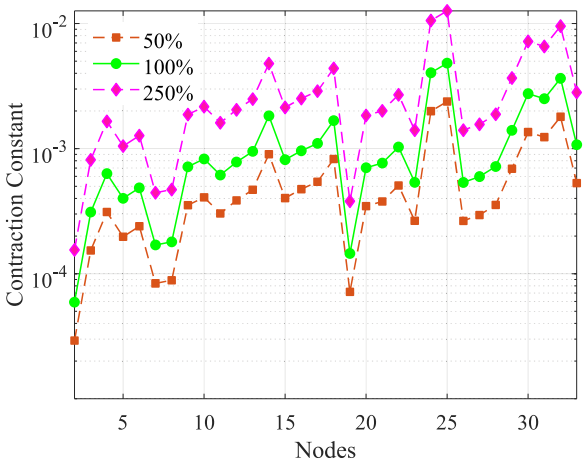

Fig. 9. Contraction constant for different loadings.

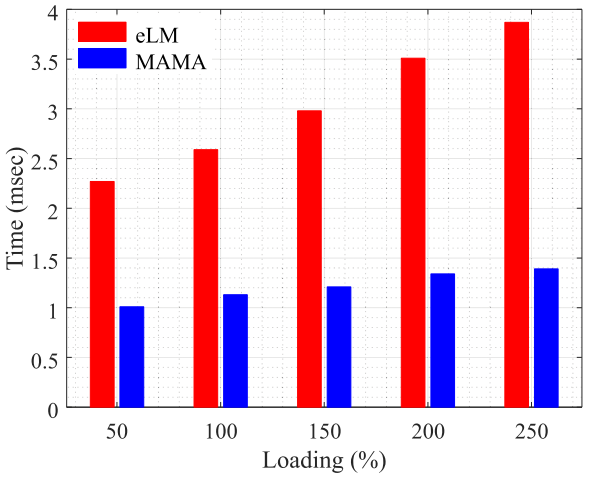

Fig. 10. Processing time.

than traditional NA if a good sparsity routine is used to load the system data and solve the equations. MANA equations are much sparser than traditional NA [21]. Moreover, NR with MANA offers much better convergence properties than NR with traditional NA, especially under ill conditions. MANA can guarantee convergence as long as the conditions established by Kantorovich's theorem are maintained [20]. It is important to highlight that the convergence range supplied by MANA is more than sufficient for practical applications, as solutions with MANA may diverge only when these constraints are violated. In [21], it was demonstrated that the MANA-NR formulation is the most robust method and requires less number of iterations compared to the fixed-point solver.

5. Conclusion

This article proposed a unique LF solver for DCDSs hosting CPLs. The proposed solver formulates the DC/DC converter models into the LF equations. The proposed method is formulated with MANA approach and is implemented with NR algorithm. The precision of the proposed method is validated with eLM and EMT results. The convergence characteristics of the proposed and the eLM methods were demonstrated with Kantorovich's theorem and BFPT, respectively, for different loadings. Results show that both methods possess convergence ranges that cover practical loading applications. However, MANA offered the best simulation speed when compared to the eLM LF solver.

Declaration of competing interest

The authors declare no conflict of interest.

Data availability

No data was used for the research described in the article.

Acknowledgments

This work was supported by the Hong Kong Research Grant Council for the Research Project under Grant 15229421.

References

[1] IEC. LVDC: electricity for the 21st century. Technical report, 2018, Available online: https://www.iec.ch/basecamp/lvdc-electricity-21stcentury [Accessed 5/10, 2022].
[2] Fairley P. DC versus AC: The second war of currents has already begun [in my view]. IEEE Power Energy Mag 2012;10(6):101–4.
[3] Van Hertem D, Gomis-Bellmunt O, Liang J. Drivers for the development of HVDC grids. In: Hvdc grids: for offshore and supergrid of the future. Hoboken, NJ, USA: Wiley; 2016, p. 3–24.
[4] Hammerstrom DJ. AC versus DC distribution systemsdid we get it right? In: 2007 IEEE power engineering society general meeting. IEEE; 2007, p. 1–5.
[5] Saeedifard M, Graovac M, Dias R, Iravani R. DC power systems: Challenges and opportunities. In: IEEE PES general meeting. IEEE; 2010, p. 1–7.
[6] Starke M, Li F, Tolbert LM, Ozpineci B. AC vs. DC distribution: maximum transfer capability. In: 2008 IEEE power and energy society general meeting-conversion and delivery of electrical energy in the 21st century. IEEE; 2008, p. 1–6.
[7] Aanesen K, Heck S, Pinner D. Solar power: Darkest before dawn. McKinsey Sustain Res Product 2012;14.
[8] Mahmoud MM. Economic applications for LED lights in industrial sectors. In: Light-emitting diodes and photodetectors: advances and future directions. 2021, p. 21.
[9] Chen Y-M, Liu Y-C, Lin S-H. Double-input PWM DC/DC converter for high-/low-voltage sources. IEEE Trans Ind Electron 2006;53(5):1538–45.
[10] AL-Nussairi MK, Bayindir R, Padmanaban S, Mihet-Popa L, Siano P. Constant power loads (cpl) with microgrids: Problem definition,stability analysis and compensation techniques. Energies 2017;10(10):1656.
[11] Purgat P, et al. Design of a power flow control converter for bipolar meshed lvdc distribution grids. In: 2018 IEEE 18th international power electronics and motion control conference. IEEE; 2018, p. 1073–8.
[12] Grisales-Noreña LF, Montoya OD, Gil-González WJ, Perea-Moreno A-J, Perea-Moreno M-A. A comparative study on power flow methods for direct-current networks considering processing time and numerical convergence errors. Electronics 2020;9(12):2062.
[13] Montoya OD, Gil-González W, Garces A. Numerical methods for power flow analysis in DC networks: State of the art, methods and challenges. Int J Electr Power Energy Syst 2020;123:106299.
[14] Taheri S, Kekatos V. Power flow solvers for direct current networks. IEEE Trans Smart Grid 2019;11(1):634–43.
[15] Javid Z, Karaagac U, Kocar I, Chan KW. Laplacian matrix-based power flow formulation for LVDC grids with radial and meshed configurations. Energies 2021;14(7):1866.
[16] Javid Z, Karaagac U, Kocar I. Improved Laplacian matrix based power flow solver for DC distribution networks. Energy Rep 2022;8:528–37.
[17] Montoya OD, Grisales-Noreña L, González-Montoya D, Ramos-Paja C, Garces A. Linear power flow formulation for low-voltage DC power grids. Electr Power Syst Res 2018;163:375–81.
[18] Montoya OD, Garrido VM, Gil-González W, Grisales-Noreña LF. Power flow analysis in DC grids: Two alternative numerical methods. IEEE Trans Circuits Syst II 2019;66(11):1865–9.
[19] Javid Z, Xue T, Karaagac U, Kocar I. Efficient graph theory based load flow solver for DC distribution networks considering DC/DC converter models. In: Presented at the 9th international conference on (PESA) power electronics systems and applications 2022, Vol. 22/9. Hong Kong; 2022, p. 7143.
[20] Javid Z, Karaagac U, Kocar I. MANA formulation based load flow solution for DC distribution networks. IEEE Trans Circuits Syst II 2023.
[21] Kocar I, Mahseredjian J, Karaagac U, Soykan G, Saad O. Multiphase load-flow solution for large-scale distribution systems using MANA. IEEE Trans Power Deliv 2013;29(2):908–15.
[22] Cetindag B, Kocar I, Gueye A, Karaagac U. Modeling of step voltage regulators in multiphase load flow solution of distribution systems using Newton's method and augmented nodal analysis. Electr Power Compon Syst 2017;45(15):1667–77.
[23] Kocar I, Karaagac U, Mahseredjian J, Cetindag B. Multiphase load-flow solution and initialization of induction machines. IEEE Trans Power Syst 2017;33(2):1650–8.
[24] Wedepohl L, Jackson L. Modified nodal analysis: An essential addition to electrical circuit theory and analysis. Eng Sci Educ J 2002;11(3):84–92.
[25] Javid Z, Xue T, Karaagac U, Kocar I. Unified power flow solver for hybrid AC/DC distribution networks. IEEE Trans Power Deliv 2023. (First revision received).